Dynamic response of transmission line conductors under downburst and synoptic winds

Haitham Aboshosha[1,2] and Ashraf El Damatty[*2]

[1]*Boundary Layer Wind Tunnel Laboratory (BLWTL), University of Western Ontario, London, Ontario, Canada*
[2]*Department of Civil and Environmental Engineering, University of Western Ontario, London, Ontario, Canada*

Abstract. In the current study, dynamic and quasi-static analyses were performed to investigate the response of multiple-spanned and single-spanned transmission line conductors under both downburst and synoptic winds considering different wind velocities and different length spans. Two critical downburst configurations, recommended in the literature and expected to cause maximum conductor reactions, were considered in the analyses. The objective of the study was to assess the importance of including the dynamic effect when predicting the conductor's reactions on the towers. This was achieved by calculating the mean, the background and the resonant reaction components, and evaluating the contribution of the resonant component to the peak reaction. The results show that the maximum contribution of the resonant component is generally low (in the order of 6%) for the multiple-spanned system at different wind velocities for both downburst and synoptic winds. For the single-spanned system, the result show a relatively high maximum contribution (in the order of 16%) at low wind velocity and a low maximum contribution (in the order of 6%) at high wind velocity for both downburst and synoptic winds. Such contributions may justify the usage of the quasi-static approach for analyzing transmission line conductors subjected to the high wind velocities typically used for the line design.

Keywords: downburst; synoptic winds; transmission line conductors; turbulence gust factor (GF)

1. Introduction

1.1 Literature review

Transmission lines (TLs) are used to carry electricity from sources of production to the distribution system. They consist of towers, conductors, ground wires and insulators. Conductors, which are responsible for transmitting the electricity, are supported by the towers through insulators. Ground wires are used as protection elements to transmit electrical charges to the ground in case of lightening. Transmission lines have been always designed to withstand forces induced by synoptic wind events. However, High Intensity Winds (HIW), in the form of downbursts or tornadoes, have not been typically considered in the design of the towers. By reviewing many cases of transmission line failures worldwide, it is revealed that more than 80% of weather-related failures of TLs are attributed to HIW as indicated by Dempsey and White (1996).

∗Corresponding author, Professor, E-mail: damatty@uwo.ca

Li (2000) reported that more than 90% of transmission line failures in Australia resulted from downburst events that are usually associated with thunderstorms. Dempsey and White (1996) also emphasized the possibility of multiple towers failure that could be triggered due to failure of a single tower. Failures that happened in Manitoba, Canada, in September 1996 and reported by McCarthy and Melsness (1996) represent a manifestation for this type of multiple tower failure. A downburst is a strong downdraft that induces an outburst of damaging winds near the ground as stated by Fujita (1990). Previous failure studies performed by Savory *et al.* (2001), Shehata and El Damatty (2008) and El Damatty and Aboshosha (2012) on different transmission towers subjected to downburst loading revealed the importance of wind forces acting on the conductors. Most of the previous attempts to analyze the behaviour or the failure of transmission lines under downburst were performed using quasi-static analysis, assuming no dynamic effects and no interaction between the line components and the wind load (Savory *et al.* 2001, Shehata *et al.* 2005, Shehata and El Damatty 2007, Darwish and El Damatty 2011). This assumption can be justified for typical towers with fundamental frequency in the order of 1 Hz or more (Holmes *et al.* 2008). However, this might not be the case for conductors which might be dynamically excited because of the proximity of their natural frequencies to the frequencies of the wind turbulence. Few attempts were done to investigate the dynamic response of the conductors. Matheson and Holmes (1981) conducted non-linear dynamic analysis of a single spanned conductor using finite difference approach. They compared the conductor response to the corresponding value obtained using the statistical approach proposed by Castenheta (1971). They found a very good agreement in the results predicted by the two approaches. Moreover, the study emphasized the effect of the aerodynamic damping in attenuating the resonant component of the response. The importance of the aerodynamic damping was also reported by Loredo-Souza and Davenport (1998). Loredo-Souza and Davenport (1998) conducted wind tunnel test of a single spanned conductor system subjected to synoptic winds. Their studies showed that, depending on the amount of aerodynamic damping, the resonant response can be as important as the background response. Researchers such as Battista *et al.* (2003) and Gani and Legeron (2010), emphasized the importance of considering the dynamic effects. On the other hand, the study conducted by Darwish *et al.* (2010) for downburst loading reported that the dynamic response was mainly due to the background component, while the resonant component had a minor effect. Two reasons could be behind their findings. The first reason is related to the assumption made regarding the spatial distribution of the turbulent component. In the study conducted by Darwish *et al.* (2010), turbulent component was extracted from a downburst that happened in June 2002, west of Lubbock, Texas, USA (Holmes *et al.* 2008). This downburst was measured using 4 anemometers installed at 4 different towers at 10 m height with horizontal spacing of 263 m. In addition, one of the towers had four other anemometers at 2, 4, 6 and 15 meter height. The total horizontal distance covered during in these measurements is 720 m, which is less than the total length of the six span conductors required to do the numerical analysis. Because of this, Darwish *et al.* (2010) relied on the turbulence extracted from one measurement point and made an assumption of a fully correlated turbulence. This assumption tend to magnify the background and the resonant responses. The second reason is related to the estimation of the aerodynamic damping. Darwish *et al.* (2010) utilized the expression for aerodynamic damping derived by Davenport (1962), which is suitable for synoptic winds. This expression requires additional modifications to account for the increase of the conductor's tensile force and the consequent increase in the conductor natural frequencies when subjected to a downburst. Neglecting this effect exaggerates the aerodynamic damping and tends to attenuate the resonant dynamic excitation. Lin *et al.* (2012) studied a single span

conductor subjected to 57 simulated downbursts. Although most of their results were in favor of neglecting the dynamic effects, some of their results were not, and therefore the authors stated the need for additional research.

2. Scope of the study

In the current study, dynamic analyses were performed to investigate the response of two different conductor systems under both downburst and synoptic winds considering different wind velocities and different length spans. The objective of the study is to assess the importance of including the dynamic effect when predicting the response of the conductors under both synoptic and downburst wind loading. Specifically, the paper focuses on the prediction of the transverse and longitudinal forces transmitted from the conductors to the tower due to these types of loading. The study considered the two conductor arrangements shown in Figs. 1(a) and 1(b). The configuration shown in Fig. 1(a) represents the case of adjacent conductors not sharing a single insulator. In this case, modeling of a single span is sufficient to predict the response of the conductors. On the other hand, Fig. 1(b) represents the case where adjacent conductors share the same insulator. Modeling multiple conductors is needed in this case because of their mutual interaction. For such cases, and according to Shehata *et al.* (2005), modeling six conductor spans, three from each side of the tower of interest, is sufficient to obtain accurate prediction for the forces transmitted from the conductors to the tower.

The paper starts by providing a description for different systems of conductors considered in the study. In addition, a detailed description of the downburst and synoptic wind fields is provided. Various steps applied to perform dynamic analyses and to obtain peak responses are then described. These steps include: (i) conducting a non-linear static analysis for the conductor system to obtain the conductor's time-dependent tension forces and displacements due to the running-mean wind velocities. These tension forces and displacements were used to calculate the time-dependent stiffness of the conductor, (ii) conducting a linear dynamic analysis under wind turbulence to calculate peak dynamic responses including resonant and background components using the time-dependent stiffness obtained in step (i), (iii) conducting a linear quasi-static analysis under wind turbulence to determine the background component alone. The results of the dynamic analysis are then presented and discussed. Finally, conclusions and recommendations obtained from this study are provided.
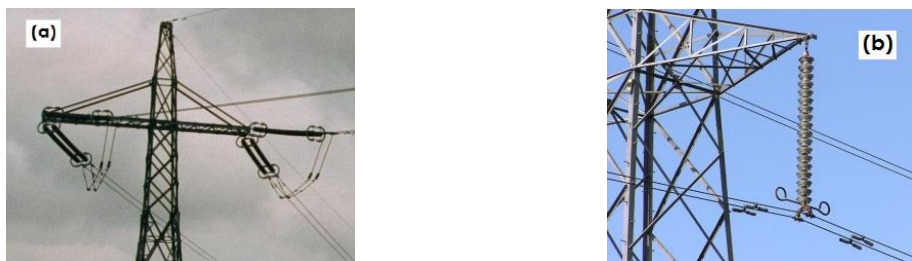

Fig. 1 Insulator used in different systems: (a)-single spanned, Wikipedia:
http://en.wikipedia.org/ wiki/Baltic Cable
(b)-six spanned, http://www.electrotechnik.net/2010/01/back-flashovers-introduction.html

3. Description of different cases considered in the analysis

A total of twelve different analysis cases were considered in this study for single-spanned and multiple-spanned conductor systems having properties summarized in Table 1. The twelve cases considered cover three loading scenarios: (i) four cases of downburst winds that cause maximum longitudinal reactions, (ii) four cases of downburst winds that cause maximum transverse reactions, (iii) four cases of synoptic winds. The cases of downbursts that cause maximum longitudinal and transverse reactions were chosen based on the recommendation of El Damatty *et al.* (2013) as will be discussed later in this section. For each of the three wind scenarios, the four cases considered cover two different mean wind velocities and two different span lengths. A summary of all the cases considered is provided in Table 2. The mean wind velocity was selected as a variable in the parametric study since it is expected to affect the aerodynamic damping, which is the main source of attenuation for the resonant component as indicated by Loredo-Souza and Davenport (1998).

Table 1 Properties of the conductor systems

Property	Value
Span Length L_x (m)	300 and 500 m
Sag Length S (m)	$L_x/30$
Elasticity Modulus $E(N/m^2)$	5.2E10
Weight W(N/m)	17.92
Projected Area in the wind direction (m^2/m)	0.022
Drag coefficient C_d according to the ASCE:74 (2010)	1.0
Cross sectional Area (m^2)	0.7E-04
Insulator Length v(m)	4.0
Average elevation (m)	43.0
Initial Tension $T_0 = W.L_x^2/8.S$ (kN)	20

Table 2 Studied cases

Case	1	2	3	4	5	6	7	8	9	10	11	12
Type*	Db_x	Db_x	Db_x	Db_x	Db_y	Db_y	Db_y	Db_y	Sy	Sy	Sy	Sy
L_x (m)	300	300	500	500	300	300	500	500	300	300	500	500
V_{ref} (m/s)	40	20	40	20	40	20	40	20	40	20	40	20

Db_x, Db_y: Downburst case for the maximum longitudinal reaction R_x (D=2.0 L_x, R=1.60 D_j and $\Theta=30^o$) and transverse reaction R_y (D=2.0 L_x, R=1.20 D_j and $\Theta=0^o$)
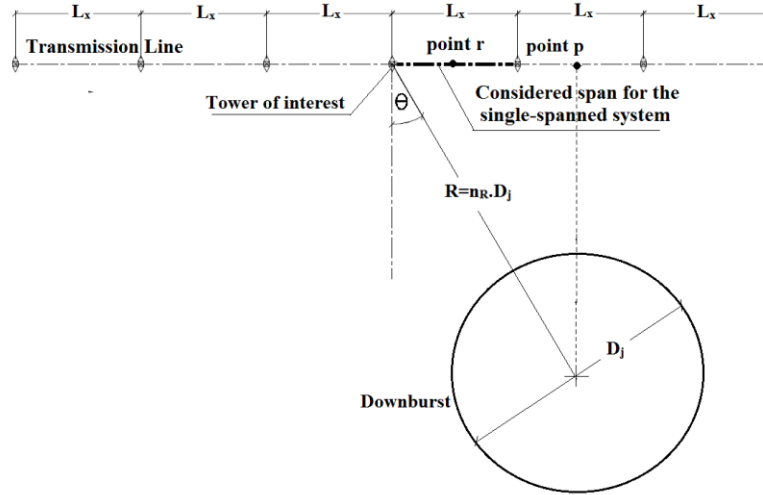Sy: Synoptic winds
V_{ref}: Reference mean velocity

Fig. 2 Downburst parameters D_j, R and Θ

At the same time, by varying the span length, the portion of the conductor affected by the correlated turbulence is expected to change and, consequently, the magnitude of the fluctuating components (background and resonant) will change. These components are influenced by the turbulent length scale in the transverse direction, L_{uv}, as will be discussed in detail in section 3.1. In the following subsections, the wind fields considered, including both the mean and turbulent components are presented.

2.1 Mean wind velocities

Wind velocities associated with downbursts and synoptic winds can be decomposed into a mean and a fluctuating component. However, the mean component associated with downbursts is different than that of synoptic winds because of its time and spatial dependency. As a result of the time dependency, it is usually named the "running-mean" or the "non-stationary mean" (Choi and Hidayat 2002, Holmes *et al.* 2008, Kwon and Kareem 2009). In the current study, the running-mean component of downbursts was extracted from the CFD simulation performed by Hangan and Kim (2007), based on the analogy between a downburst and a jet impinging to a wall (Fujita 1985). In the CFD simulation, Unsteady Reynolds Averaged Navier Stoke's (URANS) equations were solved together and the turbulence was accounted for using the Reynolds Stress Model (RSM). The running-mean component obtained from the CFD simulation was then scaled-up using the technique proposed by Shehata *et al.* (2005) to account for different event sizes and jet velocities. The mean component was evaluated at 10 points along each conductor span to account for the spatial variation. As indicated by Shehata and El Damatty (2007), and Darwish and El Damatty (2011), the running-mean velocities acting on the conductor are functions of the event size, D_j, and the downburst location relative to the conductor, which is identified by the polar coordinates, R and Θ shown in Fig. 2. According to El Damatty *et al.* (2013), an event having a jet diameter $D_j = 2$. L_x and coordinates R= 1.60 D_j and $\Theta = 30^o$ relative to the tower leads to peak longitudinal reactions at that tower. Similarly an event with the same diameter but with

relative coordinates R=1.20 D_j and $\Theta= 0^o$, leads to peak transverse reactions. In the current study, the downburst scenario considered, referring to peak longitudinal reactions, was named Db_x, while that referring to peak transverse reaction was named Db_y, as indicated in Table 2. Table 2 also summarizes the reference velocity, V_{ref}, considered in each case. This reference velocity, V_{ref}, was taken as the maximum running-mean velocity at the nearest point to the downburst centre (point "p" shown in Fig. 2). It was taken at an elevation of 43 m, which corresponds to the average conductor height. For the downburst cases, two reference velocities of 20 and 40 m/s were considered. For comparison purposes, the same two reference velocity values were assumed in the synoptic wind cases, where the mean velocities are time-independent in such cases.

2.2 Fluctuating wind velocities

The fluctuating wind velocities for both downbursts and synoptic winds can be generated numerically using the technique described by Chen and Letchford (2004) and Chay *et al.* (2006). This technique is general, which means that it can be applied for downburst winds with running-mean velocities and also for synoptic winds where the mean velocities are time independent. In this technique, the Power Spectrum Density (PSD), which describes the energy of the wind fluctuations in the frequency domain, proposed by von Karman (1948), was used to synthesize non-scaled turbulent velocities. These turbulent velocities were scaled using a modulation function. A time-dependent modulation function was chosen for the case of downbursts while a constant function was employed for synoptic winds. This was done to account for the time variation of the turbulent fluctuations with the change of the mean velocity values. The employed modulation function was taken equal to the product of the turbulence intensity, I, and the mean velocity similar to Chay *et al.* (2006). The study conducted by Holmes *et al.* (2008) showed similarity between the spectra of the synoptic and the downburst winds. As such, von Karman's PSD was used in this study for both wind types. The turbulent length scale, L_u, which is required for the PSD of von Karman, was taken equal to the event size, D_j, similar to the assumption made by Chay *et al.* (2006) for the downburst cases. Accurate estimation of the turbulent length scale, L_u, associated with downbursts requires additional research. For the cases of synoptic wind, the turbulent length scale, L_u, was calculated employing the approximate relationship $L_u=L_{uv}/0.3$, where L_{uv} is the turbulent length scale of the longitudinal fluctuations, u, along the transverse direction v. The length scale, L_{uv}, was considered equal to 52 m according to ASCE:74 (2010), assuming an open terrain. Correlations among the fluctuating components were introduced based on the coherency decay function proposed by Davenport (1986) using a coherency decay constant equal to 10, which is suitable for structural design purposes. The turbulent intensity was found to be in the order of 10% in a real downburst event as indicated by Holmes *et al.* (2008). For the case of synoptic winds, the turbulent intensity was found to be 14%, according to the AS/NZS:7000 (2010). A single averaged value of 12% was considered for both events for comparison purposes. Turbulent velocities were generated at 10 points along each conductor span to account for the spatial variation.

As a demonstration, Figs. 3 (a) and 3(b) show samples of the mean and turbulent velocities taken at point p normalized by the reference velocity, V_{ref}, for downburst case (no. 1) and for synoptic wind case (No. 9), respectively. The horizontal axis represents a time, t, non-dimensionalized by the reference velocity V_{ref} and the longitudinal length scale L_u. The figures also show the time variation of the total velocity obtained by adding the mean and turbulent velocities.
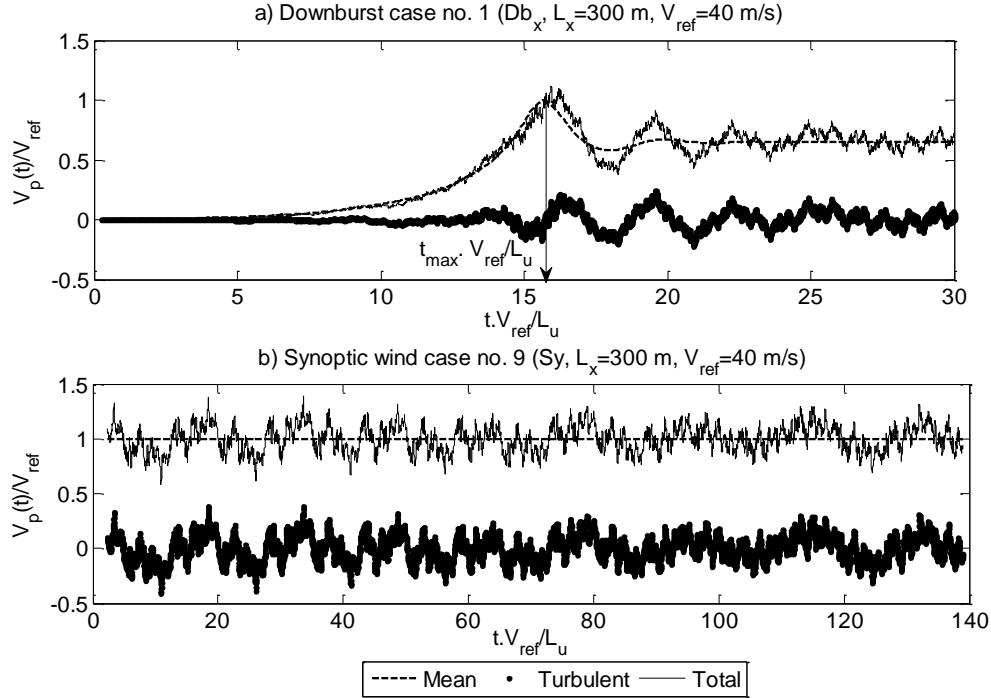
Fig. 3 Velocity time history at point p for: (a) downburst case no. 1 (Dbx, L_x=300, V_{refp}=40 m/s) (b) synoptic wind case No. 9 (Sy, L_x=300, V_{refp}=40 m/s)

4. Technique used to analyze conductor systems

Conductors and insulators are structural elements that behave non-linearly under the applied loads because of their low rigidity. This makes their dynamic analysis computationally very demanding. In order to reduce the computational demands, the dynamic analysis was conducted in the current study following the steps outlined in Fig. 4. The figure summarizes the steps of the analysis as follows: (i) the conductors were analyzed non-linearly under forces resulting from mean wind velocities - the results of this analysis provided the conductor's mean response component, M, tension forces and deformed configuration; (ii) a linear analysis was conducted to evaluate the incremental response due to fluctuating velocities, F. In this analysis, the conductor stiffness corresponding to the deformed configuration and tension forces resulting from the mean velocity analysis were employed. According to Sparling and Wegner (2007), this approach leads to a significant saving in terms of computational time without compromising the accuracy of the solution. This is mainly because of the small ratio between the fluctuating and the mean components. The fluctuating response, F, consists of the background and resonant components. In order to distinguish between the two components, a third analysis step was conducted as indicated in Fig. 4. In this step, a quasi-static analysis under the fluctuating forces was performed using the updated conductor stiffness resulting from the first analysis step to obtain the background component, B. This background component of the responses, B, was then subtracted from the fluctuating response, F, to separate the resonant component, R. By adding the velocity components

together (the mean M, the background B, and the resonant R), the total response of the conductor was evaluated. More details about the steps utilized in the analysis are given below.

Step 1: Non-linear quasi-static analysis under the mean wind

As previously mentioned, the "running mean" velocity of the downburst cases was adopted from the CFD simulation conducted by Kim and Hangan (2007), who indicated that the mean velocity has a horizontal and a vertical components. According to the findings by Kim and Hangan (2007) and Aboshosha and El Damatty (2014), the horizontal component of the mean velocity is the dominant and the vertical component can be neglected when calculating the forces acting on the conductor. This is also true for the synoptic wind cases where the mean velocities are typically in the horizontal direction. Consequently, as indicated in Fig. 5, the conductor systems were subjected to a wind load, g_y, acting in the transverse direction, Y, in addition to the conductor weight W acting in the vertical direction Z. The intensity of the distributed load, $g_y(s)$, was calculated using Eq. (1) as a function of the mean wind velocity, $V_m(s)$, at a general locations.
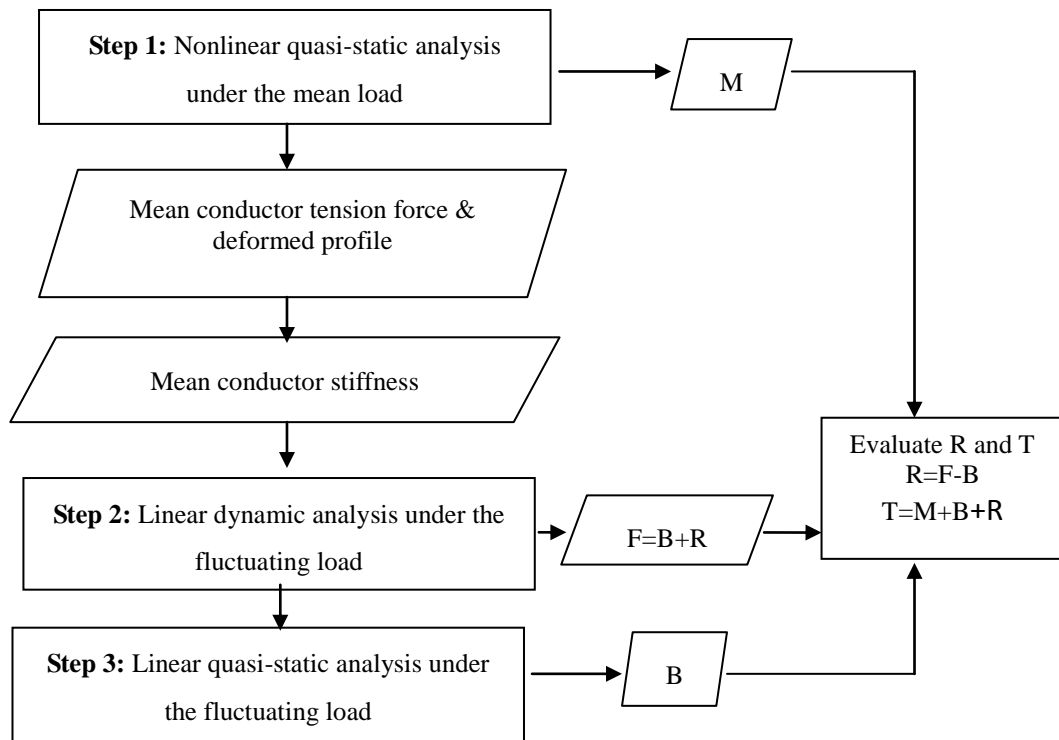
M: mean response; F: fluctuating response; B: background component;

R: resonant response; T: total response

Fig. 4 Steps of the conductor analysis

$$g_y(s) = \frac{1}{2}.\rho.C_d.V_m(s)^2.D \qquad (1)$$

where ρ is the air density which was taken equal to 1.25 kg/m³; C_d is the drag coefficient of the conductor which was taken equal to 1.0 according to the ASCE:74 (2010), D is the conductor projected area in the transverse direction per unit length. For a single bundled conductor, D is equal to the conductor diameter.

The non-linear static analyses under the mean wind load, g_y, and the conductor weight, W, were conducted using the technique developed and validated by Aboshosha and El Damatty (2014). The technique treats each conductor span as a one element, thus reduces the unknown degrees of freedom by limiting them at the connections between the insulators and the conductors.

This technique was used to evaluate the reactions, R_{xi}, R_{yi} and R_{zi} at the supports and the displacements d_{xi}, d_{yi} and d_{zi} at the conductor-insulator connecting points as illustrated in Fig. 5, where i is the number of the insulator. According to the technique, vectors of the reactions, $\{R_x\}$, $\{R_y\}$ and $\{R_z\}$ and the displacements, $\{d_x\}$, $\{d_y\}$ and $\{d_z\}$ were calculated using Eqs. (2)-(4) following the flowchart presented in Fig. 6.

$$\{R_y\} = \{R_y^F\} + [K_{yz}].\{d_y\}, \qquad \{R_z\} = \{R_z^F\} + [K_{yz}].\{d_z\} \qquad (2)$$

$$\{d_x\}^{i+1} = \{d_x\}^i + [K_x]^i.\{f_x\}^i, \qquad \{R_x\} = \left\{d_x.\frac{R_{res}}{v}\right\} \qquad (3)$$

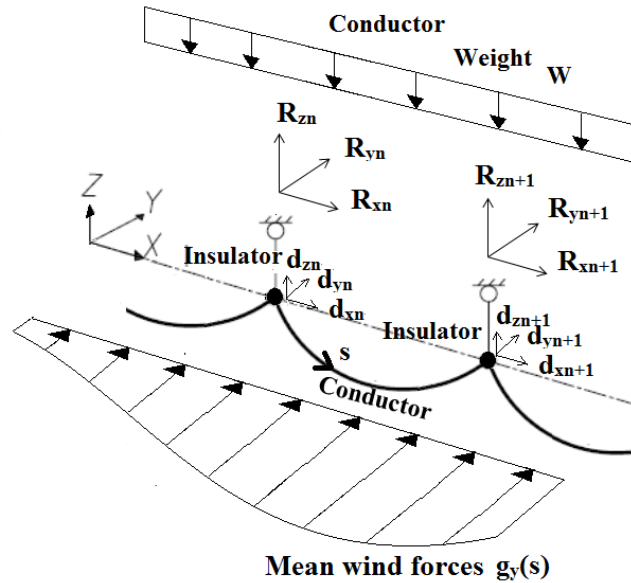$$\{d_y\} = \left\{v.\frac{R_y}{R_{res}}\right\}, \qquad \{d_z\} = \left\{v - v.\frac{R_z}{R_{res}}\right\} \qquad (4)$$
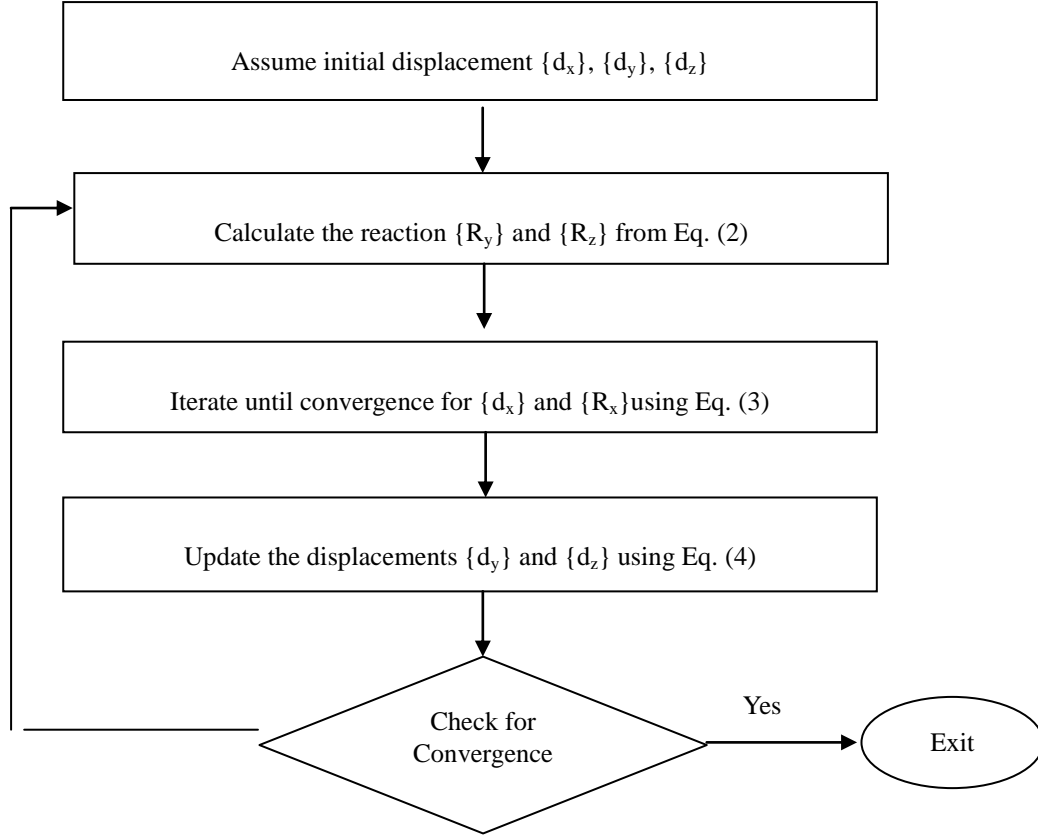

Fig. 5 Schematic illustration of the conductor-system

Fig. 6 Flow chart of the employed technique (iterate until convergence)

Where $\left\{R_y^{\ F}\right\}$, $\left\{R_z^{\ F}\right\}$ are vectors of y and z reactions considering no displacements at the connection between the conductors and the insulators, which are defined in Appendix A; $[K_{yz}]$ is the stiffness matrix to account for the p-delta effect, which is defined in Appendix A; i is the iteration number; $\{f_x\}$ is the unbalanced load vector in x-direction, which is defined in Appendix A; $[K_x]$ is the tangential stiffness matrix for x-displacements that is given in Appendix A; $\{R_{res}\}$ is the vector of the resultant forces in the insulators, $R_{res} = \sqrt{R_x^{\ 2} + R_y^{\ 2} + R_z^{\ 2}}$

As indicated in the flow chart, initial displacement vectors $\{d_x\}$, $\{d_y\}$ and $\{d_z\}$ were assumed and the corresponding reaction vectors $\{R_y\}$ and $\{R_z\}$ were calculated using Eq. (2). The horizontal displacement and reaction vectors $\{d_x\}$ and $\{R_x\}$ were calculated by iterating through Eq. (3) until no change in the results took place between two subsequent iterations. This was followed by calculating the displacement vectors $\{d_x\}$ and $\{d_y\}$ using Eq. (4), which satisfy the insulator equilibrium. The solution obtained was checked for convergence by comparing the displacement vectors obtained from the equations with the initial assumed values. If a difference greater than a chosen tolerance was found, the solution was considered not converged and the whole procedure was repeated as indicated in Fig. 6, until convergence took place.
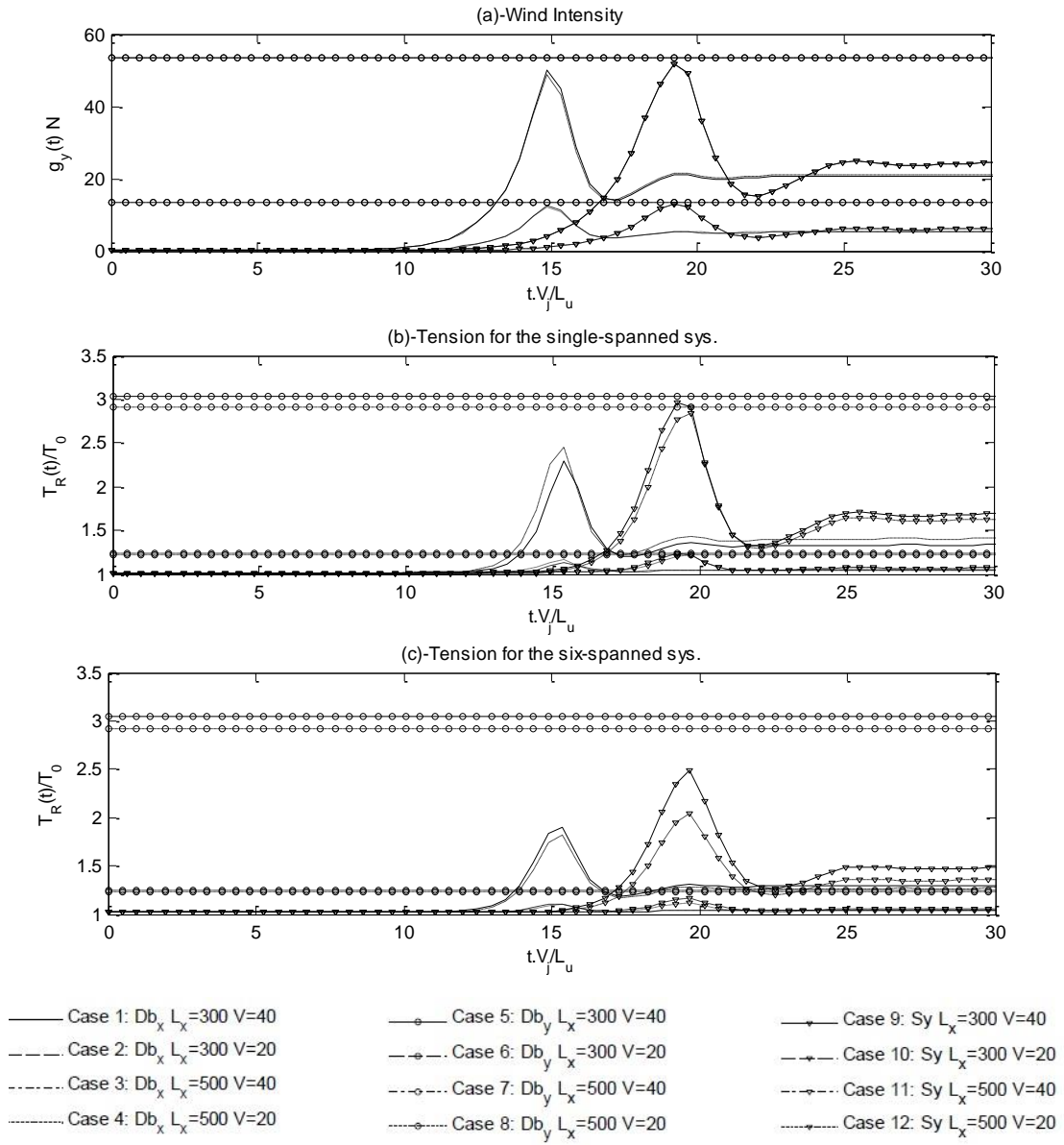
Fig. 7 Running mean time variation of the wind intensity, the tension force for the single-spanned and six-spanned systems at the right span to the tower of interest

Fig. 7(a) shows the time variation of the mean wind load intensity acting at the midpoint of the span adjacent to the tower of interest (point r indicated in Fig. 2). As shown in Fig. 7(a), the mean loads are time-dependent for the downburst cases and are time-independent for the synoptic wind cases. For the downburst cases non-linear static analyses were conducted using the technique presented in Fig. 6 at 250 time increments to capture the time history response under the time-varying mean component. One nonlinear analysis was only needed to obtain the mean response under synoptic wind. The conductor tension force and the deformed shape under the mean velocity component were obtained from the nonlinear static analysis. For the downburst cases, such parameters varied with time while they were constant for the synoptic cases. Those parameters were then used to calculate the stiffness of the conductors used in the subsequent linear dynamic analyses under the fluctuating wind component. The time history variation of the tension forces at the conductor span adjacent to the tower of interest, as obtained from the nonlinear analyses, are reported in Figs. 7(b) and 7(c) for the single and multiple spans, respectively. In these figures the tension forces are normalized by the initial tension force T_0 resulting from the conductor's own weight, $T_0 = W.L_x/8/S$.

Fig. 8 shows the time variation of the transverse displacement, d_y, and the vertical displacement, d_z, at point r for both the single and six-spanned systems. By comparing the displacements obtained from load cases 1, 3, 5, 7, 9 and 11 to those from cases 2, 4, 6, 8, 10 and 12, respectively, it is found that the increase in the mean velocity leads to an increase in the transverse displacement, d_y, and a decrease in the vertical displacement, d_z.

Figs. 7 and 8 indicate that the applied wind loads lead to significant changes in the conductor tension and its profile, which need to be accounted for in the dynamic analysis. The calculated tension forces and deformed shapes of the conductors were utilized in Step 2 to conduct the dynamic analyses.

Step 2: Linear dynamic analysis under the fluctuating wind load

As previously mentioned, linear dynamic analysis was conducted under the fluctuating wind forces. The fluctuating wind force, $F_w(t)$, acting at a nodal point representative of a tributary length L_e was calculated according to Eq. (5) where $V_m(t)$ and $v(t)$ are the mean and the turbulent velocities happening at time t, respectively.

$$F_w(t) = \rho C_d V_m(t) v(t) D L_e \tag{5}$$

The standard equation of motion of a multi-degree of freedom system subjected to a time-varying wind load is given below

$$[M]\{\ddot{u}\} + [C(t)]\{\dot{u}\} + [K(t)]\{u\} = \{F_w(t)\} \tag{6}$$

Where [M] is the mass matrix; [C(t)] is the time dependent damping matrix; [K(t)] is the time dependent stiffness matrix; $\{F_w(t)\}$ is the load vector of the fluctuating forces.

What is unique in this analysis is that both the stiffness matrix [K(t)] and the damping matrix [C(t)] were considered to be time-dependent and were evaluated based on the internal forces and deformations corresponding to the mean wind load component, which vary with time for downburst cases.
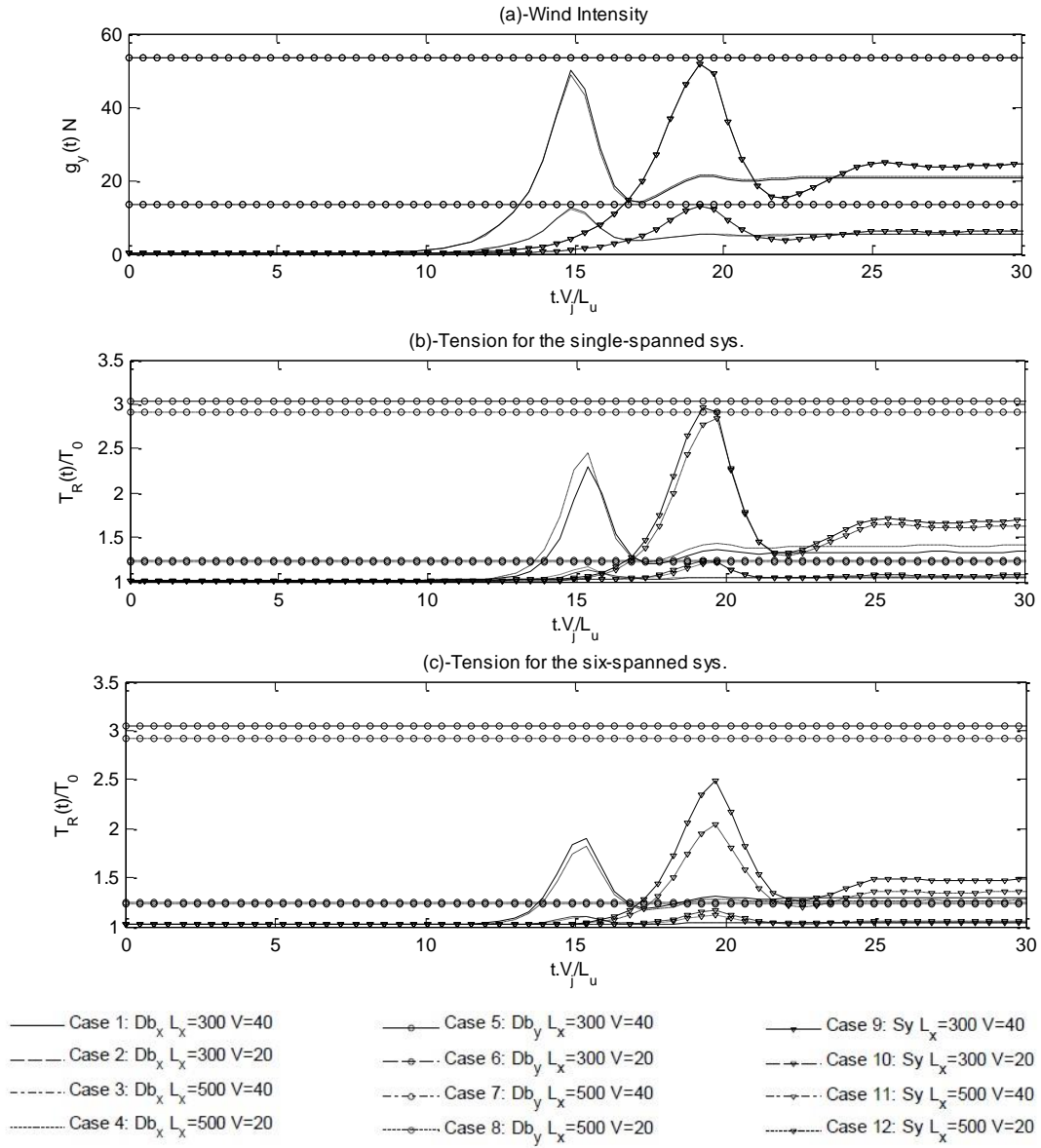
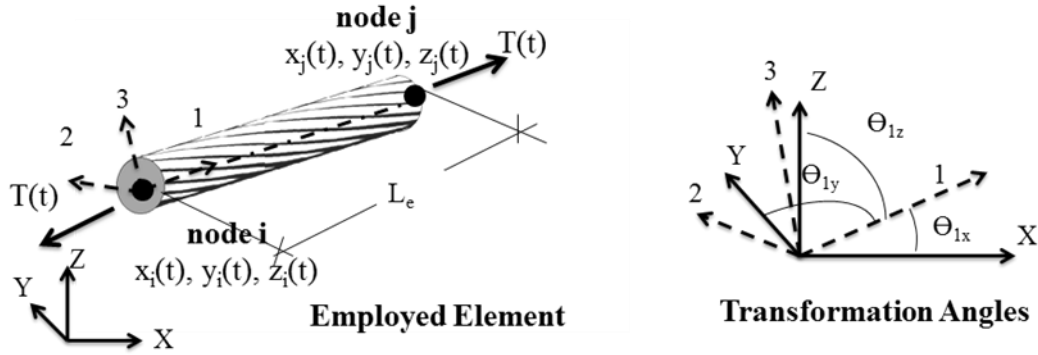Fig. 8 Time variation of the mean transverse displacement dy and vertical displacement dz at point r

Fig. 9 Employed two-noded cable element

In order to obtain the system stiffness matrix, [K(t)], each conductor span was modeled using 10 two-nodes cable elements illustrated in Fig. 9 and whose stiffness matrices, $[k_{eG}]$, in the global coordinates were calculated using Eq. (7).

$$[k_{eG}] = T_e{}^T \cdot [k_{el}] \cdot T_e$$

$$T_e = \begin{bmatrix} [R] & [0] \\ [0] & [R] \end{bmatrix}, R = \begin{bmatrix} \text{Cos}(\theta_{1x}) & \text{Cos}(\theta_{1y}) & \text{Cos}(\theta_{1z}) \\ \text{Cos}(\theta_{2x}) & \text{Cos}(\theta_{2y}) & \text{Cos}(\theta_{2z}) \\ \text{Cos}(\theta_{3x}) & \text{Cos}(\theta_{3y}) & \text{Cos}(\theta_{3z}) \end{bmatrix},$$

$$k_{el} = \begin{bmatrix} [k] & -[k] \\ -[k] & [k] \end{bmatrix}, [k] = \frac{1}{L_e} \begin{bmatrix} EA & 0 & 0 \\ 0 & T(t) & 0 \\ 0 & 0 & T(t) \end{bmatrix} \tag{7}$$

Where $[k_{el}]$ is the element stiffness matrix in the local coordinates 1, 2 and 3; T_e is the Transformation matrix; R is the directional cosine matrix; θ_{ij} is the angle between axes i and j; T(t) is the element tension force; L_e is the element length.

As indicated in Eq. (7), the element global stiffness matrix, $[k_{eG}]$, was calculated by transforming the element local stiffness matrix, $[k_{el}]$, from the local coordinates 1, 2, 3 to the global coordinates x, y and z, as illustrated in Fig. 9. This was achieved by using the transformation matrix T, which was formulated using the directional cosine matrix [R], as indicated in Eq. (7). It should be mentioned that in Eq. (7), the element length L_e and the directional cosine matrix [R] are functions of the deformed configuration of the conductor which was obtained from the non-linear analysis under mean wind forces performed in Step 1.

The mass, [M], and the damping, [C], matrices are expressed by Eqs. (8) and (9), using the lumped mass and the lumped damping at each node.

$$[M]_{3n\times3n} = \begin{bmatrix} [M_1]_{3\times3} & [0] & [0] & [0] \\ [0] & [M_2]_{3\times3} & [0] & [0] \\ : & : & \ddots & : & : \\ [0] & [0] & .. & [M_{n-1}]_{3\times3} & [0] \\ [0] & [0] & .. & [0] & [M_n]_{3\times3} \end{bmatrix}, [M_i]_{3\times3} = \begin{bmatrix} m & 0 & 0 \\ 0 & m & 0 \\ 0 & 0 & m \end{bmatrix} \quad (8)$$

$$[C]_{3n\times3n} = \begin{bmatrix} [C_{a1}]_{3\times3} & [0] & [0] & [0] \\ [0] & [C_{a2}]_{3\times3} & [0] & [0] \\ : & : & \ddots & : & : \\ [0] & [0] & .. & [C_{an-1}]_{3\times3} & [0] \\ [0] & [0] & .. & [0] & [C_{an}]_{3\times3} \end{bmatrix}, [C_{ai}]_{3\times3} = \begin{bmatrix} 0 & 0 & 0 \\ 0 & c_{ai}(t) & 0 \\ 0 & 0 & 0 \end{bmatrix} \quad (9)$$

Where n is the number of nodes, which is equal to 10 x (nSpan+1), where nSpan is the number of spans; $[M_i]$, $[C_{ai}]$ are the mass and damping matrices for node i; m is the nodal mass which is equal to $W.L_x /(20.g)$ for the first and last nodes and equal to $W.L_x /(10.g)$ for other nodes, where g is the gravitational acceleration which is equal to 9.81 m/s^2 , $c_{ai}(t)$ is the damping coefficient at node i.

According to Matheson and Holmes (1981) and Loredo-Souza and Davenport (1998), the aerodynamic damping of the conductor system is the dominant source of damping and plays a major role in attenuating the resonant component. Davenport (1962) proposed an expression for the aerodynamic damping ratio, ζ_a, based on the modal analysis procedure. Since the mode shapes are expected to change with time as a result of the variation of the conductor's tension force and nodal coordinates with time, Davenport's expression cannot be used directly. Therefore, an expression for the time-dependent damping coefficient per each node, c_{ai}, was developed in the current study as follows:

• A conductor segment with a length L_e, as shown in Fig. 10, was considered. The segment moved with a velocity $\dot{u}_{iy}$ in the transverse y-direction and was subjected to an incoming wind with a mean velocity, V_{mi}. The drag force applied on the segment due to the incoming mean wind velocity, F_{mi}, and the conductor movement can be expressed by Eq. (10).

$$F_{mi}(t) = \frac{1}{2}\rho.C_d.D.L_e.\left(V_{mi}(t) - \dot{u}_{iy}(t)\right)^2 \quad (10)$$

• This drag force, $F_{mi}(t)$, was expanded in Eq. (11) as the subtraction of the aerodynamic damping force, $F_{idair}(t)$, due to conductor movement in the wind direction, from the drag force due to the mean incoming wind, $F_{miw}(t)$. It should be mentioned that in Eq. (11) the conductor velocity, $\dot{u}_{iy}(t)$, is typically much smaller than the incoming wind velocity, $V_i(t)$, and thus the quadratic term of the conductor velocity can be neglected.

$$F_{mi} = F_{miw} - F_{idair} = \frac{1}{2}\rho.C_d.D.L_e.V_{mi}(t)^2 - \rho.C_d.D.L_e.V_{mi}(t).\dot{u}_{iy}(t) \quad (11)$$

• The aerodynamic damping force, $F_{idair}(t)$, was equated to the viscous damping force as expressed by Eq. (12), and the damping coefficient c_{ai} was accordingly evaluated using   Eq. (13).
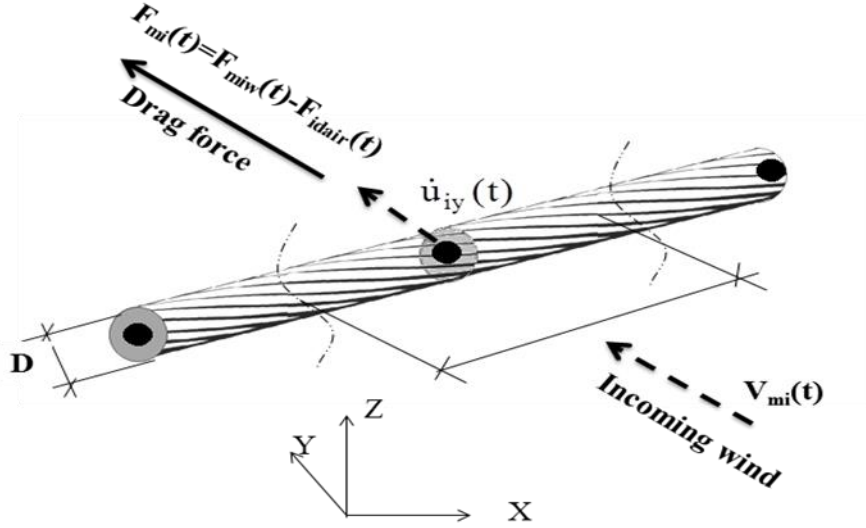
Fig. 10 Drag force at node i due to incoming wind

$$F_{idair} = \rho.C_d.D.L_e.V_i(t).\dot{u}_{iy}(t) = c_{ai}(t).\dot{u}_{iy}(t) \tag{12}$$

$$c_{ai}(t) = \rho.C_d.D.L_e.V_i(t) \tag{13}$$

where, $c_{ai}(t)$ is the diagonal element of the damping matrix $[C_{ai}]_{3\times3}$ defined in Eq. (9).

Dynamic analyses were performed using the Newmark's (Bathe 1996) step by step integration technique. This in-house program was developed to overcome some limitations found in most of the commercial finite element software. For example, most of the available software do not allow defining time dependent damping forces as required in the current study. Also, most of commercial software do not have the option of conducting the analyses under the total wind load into two steps as done in the current study. This will require a significant computational time compared with the two steps approach (Sparling and Wegner 2007). The in-house program was validated by employing it to analyze the six-spanned conductor system subjected to downburst load (case no. 4), and comparing the resulting reaction responses with the corresponding values obtained using SAP2000 CSI (2010). A constant damping ratio of 5% for the first two modes was considered in this example in order to be able to solve the problem within the capability of the commercial code.

Fig. 11(a) shows the time histories of the total and the fluctuating transverse reactions R_y obtained from the in-house and the SAP 2000 analyses. Similar time histories for the longitudinal reactions R_x are provided in Fig. 11(b). The figures show a very good agreement between the two sets of analyses. In order to obtain a more detailed comparison, the time-dependent mean and root mean square (r.m.s.) components were calculated and were plotted in Fig. 11(c) and (d). As shown in the figures, both the mean and the r.m.s. components obtained from the developed in-house program are in an excellent agreement with those obtained from the SAP 2000 results.

The developed numerical model was also validated under synoptic wind by analyzing the single-spanned conductor system considered by Matheson and Holmes (1981) and described in Table 3. Table 4 summarizes the mean and r.m.s. conductor reactions obtained using the in-house

program and those evaluated by Matheson and Holmes (1981) using full non-linear dynamic analysis. As shown from the table, reactions obtained from the in-house program are in an excellent agreement with those obtained by Matheson and Holmes (1981).

These validations provide confidence in the accuracy of the developed in-house code.

Step 3: Quasi-static linear analysis under the fluctuating wind

As mentioned earlier, a quasi-static analysis of the conductor systems under the fluctuating wind was conducted in order to distinguish between the background and resonant components. The background component of the response was obtained by doing a static analysis through solving Eq. (14). This was then subtracted from the total fluctuating component to identify the resonant component.
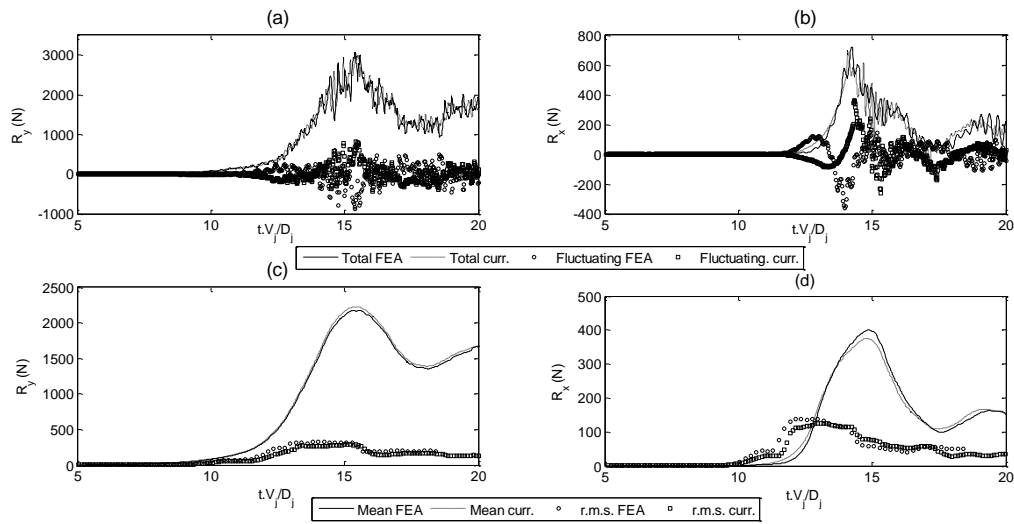

Fig. 11 Comparison between the results of the in-house program and FEA (a) time history of R_x (b) time history of R_y (c) running R_y components (d) running R_x components

Table 3 Considered single-spanned system for validating the in-house program

Property	Value
Cable Layout	Single span
Turbulent Intensity	0.15
mass (kg/m')	1.69
Projected area (m^2/m')	0.0293
Span (m)	300
Sag (m)	6.78

Table 4 Transverse reaction obtained using the in-house program and non-linear dynamic analysis (Matheson and Holmes 1981)

V_{ref}	Current technique (kN)		Matheson and Holmes 1981 (kN)		Difference %	
(m/s)	mean	r.m.s	mean	r.m.s	mean	r.m.s
10	0.267	0.051	0.261	0.0492	2%	3%
20	1.066	0.193	1.04	0.201	3%	-4%
30	2.399	0.468	2.35	0.458	2%	2%

$$[K(t)]\{u\} = \{F_w(t)\} \tag{14}$$

where $\{F_w(t)\}$ is the fluctuating load vector due to the wind load; $[K(t)]$ is the time dependent stiffness matrix obtained using the conductor tension force and the location resulting from the quasi-static analysis under the mean loads

5. Results of the dynamic analyses

The three steps discussed above in section no. 3 were followed to analyze the conductor systems under the twelve wind cases summarized in Table 2. Reactions of the single-spanned system at the left tower, R_{x1} and R_{y1}, and those for the six-spanned system at the intermediate tower, R_{x6} and R_{y6}, in the longitudinal and the transverse directions, respectively, were calculated and plotted in Figs. B1-12 presented in Appendix B. The figures report the mean, the background and the resonant components, in addition to the overall response obtained from the summation of those three components. The reported reactions were normalized using the maximum mean reaction components (R_{y1m}^* and R_{x1m}^*) for the single-spanned system and (R_{y6m}^* and R_{x6m}^*) for the six spanned system. Also, the longitudinal reactions (R_{x1} and R_{x6}) reported in the figures were normalized on the right scale using the maximum mean transverse reactions (R_{y1m}^* or R_{y6m}^*), respectively. This is to allow comparing the longitudinal reactions to the transverse reactions and, thus identifying the cases where the longitudinal reactions are critical. It should be mentioned that for the cases of synoptic wind, the mean response was used for the scaling instead of the maximum mean response since the mean response does not vary with time. Also, for the cases of synoptic winds and the cases of downbursts corresponding to the maximum transverse reactions, the mean longitudinal reaction for the six spanned system, R_{x6}, is equal to zero due to symmetry and, thus was not used in the normalization.

In order to assess the dynamic effect, responses shown in Fig. B1-B12, located in Appendix B, were used to calculate the Gust Factor, GF, defined in Eq. (15) as the ratio between the peak responses to the maximum-mean responses. Two gust factors were calculated based on how the peak responses are defined: (1) the first is named the dynamic gust factor, GF_{Dy}, where the peak

responses result from the contribution of the mean, background and resonant components. (2) The second is named the quasi-static gust factor, $GF_{QS,}$ where the contribution of the mean and the background components are only considered in calculating the peak responses.

$$GF = \frac{r_p}{\overline{r}_{max}}$$

(15)

where:

r_p : Peak response

$\overline{r}_{max}$: Maximum mean response for the downburst winds or mean response for the synoptic winds

Table 5 Gust factors for the different wind cases

Resp.	Case	Downburst-(Peak R_x)			Case	Downburst-(Peak R_y)			Case	Synoptic Winds		
Type		GF_{Dy}	GF_{QS}	$Cont_R\%$		GF_{Dy}	GF_{QS}	$Cont_R\%$		GF_{Dy}	GF_{QS}	$Cont_R\%$
R_{y1}	1: L300 V 40	1.27	1.22	3.91	5: L300 V 40	1.40	1.36	3.01	9: L300 V 20	1.38	1.32	4.20
R_{x1}		1.27	1.21	4.57		1.59	1.53	3.94		1.49	1.42	5.26
R_{y6}		1.31	1.26	3.76		**1.32**	**1.27**	**3.68**		1.42	1.33	6.62
R_{x6}		**1.18**	**1.15**	**2.92**		**	**	1.96		**	**	11.52
R_{y1}	2: L300 V 20	1.27	1.22	3.76	6: L300 V 20	1.40	1.36	2.54	10: L300 V 20	1.36	1.32	3.14
R_{x1}		1.36	1.21	11.29		1.91	1.63	14.87		1.74	1.57	9.88
R_{y6}		1.27	1.25	1.63		**1.30**	**1.27**	**2.08**		1.41	1.32	6.24
R_{x6}		**1.14**	**1.11**	**2.77**		**	**	17.68		**	**	5.79
R_{y1}	3: L500 V 40	1.30	1.25	4.23	7: L500 V 40	1.25	1.21	3.27	11: L300 V 40	1.42	1.36	3.75
R_{x1}		1.37	1.32	3.22		1.27	1.25	1.83		1.48	1.39	6.02
R_{y6}		1.18	1.18	0.72		**1.26**	**1.24**	**1.54**		1.42	1.37	3.55
R_{x6}		**1.15**	**1.14**	**0.82**		**	**	1.70		**	**	9.81
R_{y1}	4: L500 V 40	1.28	1.25	2.73	8: L500 V 40	1.25	1.21	3.08	12: L500 V 40	1.42	1.36	4.36
R_{x1}		1.35	1.26	6.76		1.32	1.24	6.10		1.85	1.55	16.49
R_{y6}		1.20	1.18	1.78		**1.25**	**1.24**	**1.34**		1.40	1.36	2.90
R_{x6}		**1.22**	**1.14**	**6.15**		**	**	1.24		**	**	4.74

GFs in bold correspond to the peak reaction caused by the considered downburst size and location

Both the dynamic and the quasi-static gust factors, GF_{DY} and GF_{QS}, are provided in Table 5 for the twelve considered cases. The contribution of the mean, $Cont_M$, background, $Cont_{BG}$, and resonant, $Cont_R$, components to the peak responses were calculated using Eq. (16) and are plotted in Fig. 12.

$$Cont_M = \frac{1}{GF}, \quad Cont_{BG} = \frac{GF_{QS}-1}{GF}, \quad Cont_R = \frac{GF-GF_{QS}}{GF} \quad (16)$$

The contribution of the resonant component, $Cont_R$, which is reported in Table 5, represents the error in the estimated peak response when the dynamic effect is not considered. High values of such a contribution imply the importance of conducting dynamic analysis. The following remarks points can be made by in view of the values of $Cont_R$ calculated for different cases:

(i)   The contribution, $Cont_R$, to the peak longitudinal reaction R_{x1} for the single-spanned system reached a maximum value of 15% for the downburst cases and 17% for the synoptic wind cases when considering the low reference velocity (20 m/s). The contribution reached a maximum value of 4.5% and 6% for the downburst and the synoptic wind cases, respectively, for the high reference velocity (40 m/s). These results indicate that dynamic analysis is recommended to analyze single-spanned system subjected to low velocities for both downburst and synoptic winds. The contribution of the resonant component, $Cont_R$, to the peak transverse reaction R_{y1} was generally low and less than 5% under both the downburst and the synoptic wind cases.

(ii)   The contribution to the peak transverse reaction R_{y6} for the six-spanned system was in the order of 4% or less for the downburst cases and in the order of 6% for the synoptic wind cases. Also, the contribution to the peak transverse reaction R_{x6} of the six-spanned system was in the order of 6% or less for the downburst cases causing maximum longitudinal reactions (cases 1-4). These low contributions imply that conducting dynamic analysis may not be necessary for estimating the peak reactions for the six-spanned system.

By investigating the values of the GFs summarized in Table 5, it was found that for the twelve studied cases, GFs of both the longitudinal and transverse reactions for the single spanned system, R_{x1} and R_{y1}, were larger than those for the six spanned system, R_{x6} and R_{y6}. This is because correlated fluctuations characterized by the length scale, L_{uv}, cover a higher percentage of the conductor length for the single spanned system than that for the six spanned system. According to Davenport (1993), cases of high ratio of the turbulence length scale L_{uv} to the system length have more correlated fluctuations than those of low ratios.

In Figs B1-12, located in Appendix B, time histories of the reactions were normalized by the maximum mean component for each case. This allows visualizing the difference between the peak reactions and their mean components caused by the wind turbulence. In order to compare the responses obtained from the 12 cases, a general normalization using a force, $g_{yp}.L_x$, was applied to the reaction responses, as shown in Fig. 13. This normalization force is equal to product of the wind intensity applied at point p, g_{yp}, and expressed by Eq. (17), and the span length L_x. This force, $g_{yp}.L_x$, represents the maximum mean transverse force acting on the towers assuming a uniform distribution of the wind load.

$$g_{yp}^* = \frac{1}{2}\rho.C_d.V_{ref}^2.D \quad (17)$$

Fig. 13 shows the normalized peak reactions for the twelve considered cases. As shown in the figure, the maximum downburst peak transverse reactions R_{y1p} and R_{y6p} and longitudinal reaction

R_{x1p} are associated with case no. 5 (Db_y: L_x=300 m, V_{refp}=40 m/s) and are equal to 70%, 125% and 390% of the force $g_{yp}.L_x$, respectively.   The maximum downburst peak longitudinal reaction R_{x6p} occurs at case no. 3 (Db_x: L_x=500 m, V_{refp}=40 m/s) and is equal to 45% of the force $g_{yp}.L_x$. As indicated from those values, the developed longitudinal peak reactions, R_{x1p} and R_{x6p} can be significantly high and, accordingly, should be included in the design of the line.
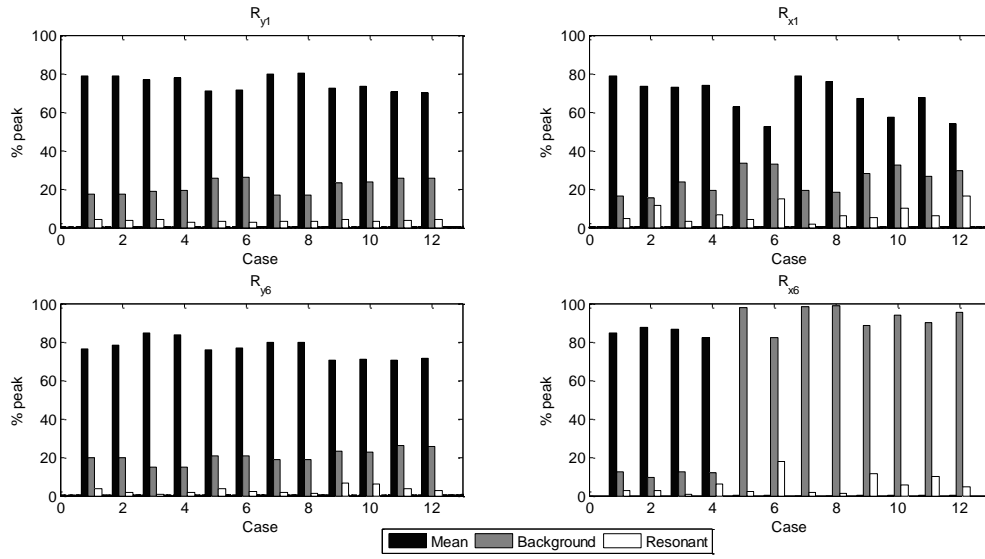

Fig. 12 Contribution of different components in the peak responses
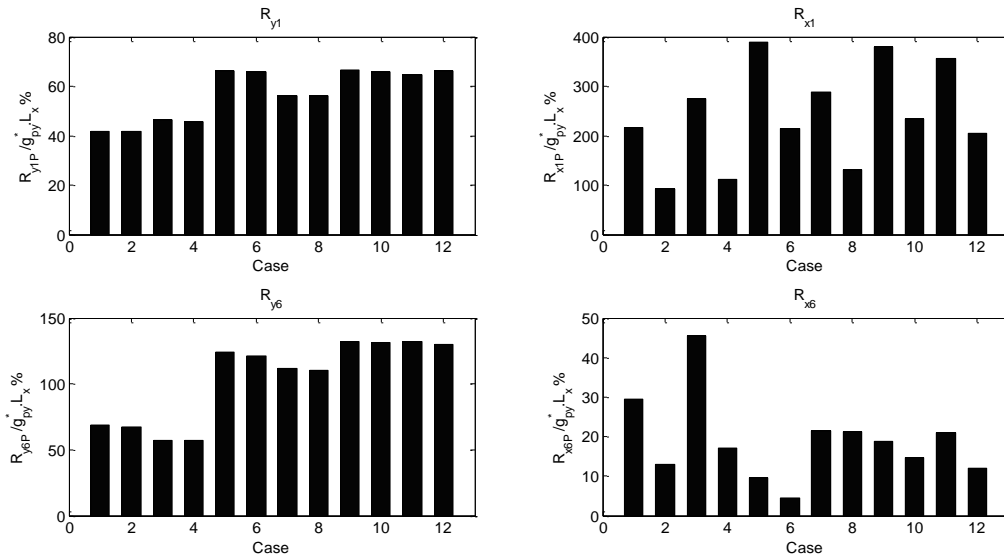
Fig. 13 Normalized peak reactions

5. Conclusions

Dynamic analyses of single-spanned and multiple-spanned conductor systems were performed in the current study. The study included twelve different cases with variation in the wind type, the mean wind velocity and the span length. Downburst and synoptic winds were used as the wind types. Two downburst loading scenarios causing maximum longitudinal conductor reaction, D_{bx}, and maximum transverse conductor reaction, D_{by}, were considered. Two mean wind velocities, (V_{ref} =20 and 40 m/s) and two span lengths, (L_x=300 and 500 m) were assumed in the analyses. A number of 6 spans (three on each side to the tower of interest) was considered in the study to model the multiple-spanned system based on a recommendation from the literature. The analyses of the two systems were conducted to obtain the longitudinal and the transverse reactions at the intermediate tower of the multiple-spanned system and at the left tower for the single spanned system.

Mean, background and resonant responses are evaluated from the analyses. The ratio between the peak responses to the maximum mean responses, defined as the Gust Factor (GF), was calculated using both the dynamic analysis, $GF_{Dy,}$ and the static analysis, GF_{QS}. The contributions of the different components to the peak response were calculated and the following conclusions were drawn:

(i)   The contribution, $Cont_R$, to the peak longitudinal reaction R_{x1} for the single-spanned system reached a relatively high maximum value (in the order of 16%) for downburst and synoptic wind cases when considering the low reference velocity (20 m/s). Under the high reference velocity (40 m/s), the contribution $Cont_R$, reached a relatively low maximum value (in the order of 5 %) for both downburst and synoptic wind cases. These results indicate that dynamic analysis is recommended to analyze single-spanned system subjected to downbursts and synoptic winds with low reference velocities.

(ii)   The maximum contribution to the peak transverse reaction R_{y6} and to the peak longitudinal reaction R_{x6} for the six-spanned system was found in the order of 5% and 6%, respectively, for both downburst and synoptic wind cases. These low contributions imply that conducting dynamic analysis may not be necessary for estimating the peak reactions for the six-spanned system.

(iii)   Gust factors of both the longitudinal and the transverse reaction for the single-spanned system were larger than those for the six-spanned system. This is because correlated fluctuations characterized by the length scale, L_{uv}, cover a higher percentage of the conductor length for the single-spanned system than that for the six-spanned system.

(iv)   Maximum peak transverse reactions for the single-spanned system, R_{y1p} and the six-spanned, system R_{y6p}, were found to be equal to 70%, 125% of the force $g_{yp}^{*}.L_x$. The maximum peak longitudinal reaction for the single spanned system, $R_{x1p,}$, and the six spanned system, R_{x6p}, were found to be equal to 390% and 45 % of the force $g_{yp}^{*}.L_x$, respectively. As indicated from the values, the developed longitudinal reactions in the two systems can be significant and should be included in the line design.

Acknowledgments

research.

References

Aboshosha, H. and El Damatty, A. (2014), "Effective technique to analyze transmission line conductors under high intensity winds", *Wind Struct.*, **18**(3), 235-252.

ASCE (2010), *Guide lines for electrical transmission line structural loading*, ASCE Manuals and Reports on Engineering Practice, 74.

Australian Standard / New Zealand Standard AS/NZS: 7000 (2010), *Overhead line design - Detailed procedures*, Standards Australia Limited / Standards New Zealand, North Sydney, Australia.

Bathe, K.J. (1996), *Finite Element Procedures in Engineering Analysis*, Prentice-Hall, Englewood Cliffs, New Jersey.

Battista, R., Rodrigues, R. and Pfeil, M. (2003), "Dynamic behavior and stability of transmission line tower under wind forces", *J. Wind Eng. Ind. Aerod.*, **91**(8), 1051-1067.

Castenheta, M.N. (1970), *Dynamic behavior of overhead power lines subject to the action of wind*, CIGRE Report 2208.

Chay, M., Albermani, F. and Wilson, R. (2006), "Numerical and analytical simulation of downburst wind loads", *Eng. Struct.*, **28**, 240-254.

Chen, L. and Letchford, C. (2004), "A deterministic-stochastic hybrid model of downburst and its impact on a cantilevered structure", *Eng. Struct.*, **26**(5), 619-629.

Choi, E.C.C. and Hidayat, F.A. (2002), "Dynamic response of structures to thunderstorm winds", *Prog. Struct. Eng. Mech.*, **4**, 408-416.

Computer and Structures, Inc. (2010), *SAP2000 V.14- CSI Analysis Reference Manual*, Berkeley, California, USA.

Darwish, M. and El Damatty, A. (2011), "Behavior of self supported transmission line towers under stationary downburst loading", *Wind Struct.*, **14**(5), 481-498.

Darwish, M., El Damatty, A. and Hangan, H. (2010), "Dynamic characteristics of transmission line conductors and behaviour under turbulent downburst loading", *Wind Struct.*, **13**(4), 327-346.

Davenport, A.G. (1962), "Buffeting of a suspension bridge by storm winds", *J. Struct. Div. - ASCE*, **88**(3), 233-264.

Davenport, A.G. (1986), "The dependence of wind load upon meteorological parameters", *Proceedings of the International Seminar on Wind Effects on Buildings and Structures*, Toronto, Canada: University of Toronto Press.

Davenport, A.G. (1993), "How can we simplify and generalize wind loads?", Presented at the Third Asia-Pacific Symposium on Wind Engineering. December 13-15, Hong-Kong, Keynote Lecture.

Dempsey, D. and White, H.B. (1996), "Winds wreak havoc on lines", *T&D World Mag.*, **48**(6), 32-42.

El Damatty, A. and Aboshosha, H. (2012), "Capacity of electrical transmission towers under downburst loading", *Proceedings of the 1st Australasia and South-East Asia Structural Engineering and Construction Conference*, Perth, Australia, Nov 28-Dec 2, 2012.

El Damatty, A., Hamada, A. and Alawady, A. (2013), "Development of critical load cases simulating the effect of downbursts and tornados on transmission line structures", Key note lecture on the 8th Asia-Pacific Conference on Wind Engineering, APCWE8, Chennai, India. December 10-14 2013.

Fujita, T.T. (1985), *The downburst microburst and macroburst*, University of Chicago, Department of Geophysical Sciences.

Fujita, T.T. (1990), "Downbursts: meteorological features and wind field characteristics", *J. Wind Eng. Ind. Aerod.*, **36**(1), 75-86.

Gani, F. and Legeron, F. (2010), "Dynamic response of transmission lines guyed towers under wind loading", *Can. J. Civ. Eng.*, **37**(3), 450-465.

Hangan, H. and Kim, J. (2007), "Numerical simulations of impinging jets with application to downbursts", *J. Wind Eng. Ind. Aerod*., **95**(4), 279-298.

Holmes, J., Hangan, H., Schroeder, J., Letchford, C. and Orwig, K. (2008), "A forensic study of the Lubbock-Reese downdraft of 2002", *Wind Struct*., **11**(2), 137-152.

Kwon, D. and Kareem, A. (2009), "Gust-front factor: new framework for wind load Effects on structures", *J. Struct. Eng. - ASCE*, **135**(6), 717-732.

Li, C.Q. (2000), "A stochastic model of severe thunderstorms for transmission line design", *Probabilist. Eng. Mech*., **15**, 359-364.

Lin, W., Savory, E., McIntyre, R., Vandelaar, C. and King, P. (2012), "The response of an overhead electrical power transmission line to two types of wind forcing", *J. Wind Eng. Ind. Aerod*., **100**(1), 58-69.

Loredo-Souza, A. and Davenport, A. (1998), "The effects of high winds on transmission lines", *J. Wind Eng. Ind. Aerod*., **74-76**, 987-994.

Matheson, M.J. and Holmes, J.D. (1981), "Simulation of the dynamic response of transmission lines in strong winds", *Eng. Struct*., **3**, 105-110.

McCarthy, P. and Melsness, M. (1996), *Severe weather elements associated with September 5, 1996 hydro tower failures near Grosse Isle*, Manitoba, Canada. Manitoba Environmental Service Centre, Environment Canada.

Savory, E., Parke, G., Zeinoddini, M., Toy, N. and Disney, P. (2001), "Modelling of tornado and microburst-induced wind loading and failure of a lattice transmission tower", *Eng. Struct*., **23**, 365-375.

Shehata, A. and El Damatty, A. (2007), "Behaviour of guyed transmission line structures under downburst wind loading", *Wind Struct*., **10**(3), 249-268.

Shehata, A., El Damatty, A. and Savory, E. (2005), "Finite element modeling of transmission line under downburst wind loading", *Finite Elem. Anal. Des*., **42**(1), 71-89.

Shehata, A. and El Damatty, A. (2008), "Failure analysis of a transmission tower during a microburst", *Wind Struct*., **11**(3), 193-208.

Sparling, B. and Wegner, L. (2007), "Estimating peak wind load effects in guyed masts", *Wind Struct*., **10**(4), 347-366.

Von Karman, T. (1948), "Progress in the statistical theory of turbulence", *Proceedings of the National Academy of Sciences of the United States of America*, 34(11), 530-539.

JH

Appendix A

Definition for the reaction vectors $\{R_y^F\}$ and $\{R_z^F\}$ and for the matrix $[K_{yz}]$

$$\{R_y^F\} = \left\{\frac{M_{gyA?}}{L_x} \quad \frac{M_{gyB?}+M_{gyA?}}{L_x} \quad \frac{M_{gyB?}+M_{gyA?}}{L_x} \quad .. \quad \frac{M_{gyB'Nd-}+M_{gyA'Nd-}}{L_x} \quad \frac{M_{gyB'Nd-}}{L_x}\right\}^T$$

,
$$\{R_z^F\} = W.L_x\left\{\frac{1}{2} \quad 1 \quad 1 \quad .. \quad 1 \quad \frac{1}{2}\right\}^T$$

$$[K_{yz}] = \begin{bmatrix} \dfrac{T_1}{L_x} & -\dfrac{T_1}{L_x} & 0 & 0 & .... & 0 \\[2mm] -\dfrac{T_1}{L_x} & \dfrac{T_1}{L_x}+\dfrac{T_2}{L_x} & -\dfrac{T_2}{L_x} & 0 & .... & 0 \\[2mm] 0 & -\dfrac{T_2}{L_x} & \dfrac{T_2}{L_x}+\dfrac{T_3}{L_x} & -\dfrac{T_3}{L_x} & .... & 0 \\[2mm] \vdots & \vdots & \vdots & \vdots & \ddots & \vdots \\[2mm] 0 & 0 & 0 & -\dfrac{T_{Nd-2}}{L_x} & \dfrac{T_{Nd-2}}{L_x}+\dfrac{T_{Nd-1}}{L_x} & -\dfrac{T_{Nd-1}}{L_x} \\[2mm] 0 & 0 & 0 & 0 & -\dfrac{T_{Nd-1}}{L_x} & \dfrac{T_{Nd-1}}{L_x} \end{bmatrix}$$

where M_{gyAj}, M_{gyBj} is the moment at the left and right ends of span no. j due to the applied load g_y; N_d is the number of conductor-insulator connections; T_j is the tension force is span j; L_x is the span length.

Definition for the unbalanced load vector, $\{f_x\}_{Ndx1}$, and the tangential stiffness matrix, $[K_x]_{NdxNd}$, in x-direction

$$\{f_x\}_{Ndx1} = \left\{\begin{array}{c} T_1 - d_{x1}\dfrac{R_{res1}}{V} \\[3mm] T_2 - T_1 - d_{x2}\dfrac{R_{res2}}{V} \\[3mm] \vdots \\[1mm] \vdots \\[3mm] T_{Nd-1} - T_{Nd-2} - d_{xNd-1}\dfrac{R_{resNd-1}}{V} \\[3mm] T_{Nd-1} - d_{xNd}\dfrac{R_{resNd}}{V} \end{array}\right\}$$

$$[K_x] = \begin{bmatrix} \dfrac{R_{res?}}{V} + C_1 & -C_1 & 0 & 0 & .. & 0 \\ -C_1 & C_1 + \dfrac{R_{res?}}{V} + C_2 & -C_2 & 0 & .. & 0 \\ 0 & -C_2 & C_2 + \dfrac{R_{res?}}{V} + C_3 & -C_3 & .. & 0 \\ \vdots & \vdots & \vdots & \ddots & \vdots & \vdots \\ 0 & 0 & .. & -C_{Nd-2} & C_{Nd-2} + \dfrac{R_{res\,Nd-}}{V} + C_{Nd-1} & -C_{Nd-1} \\ 0 & 0 & .. & 0 & -C_{Nd-1} & C_{Nd-1} + \dfrac{R_{res\,Nd}}{V} \end{bmatrix}$$

where C_n is defined below; V: insulator length; d_{xJ} is the x-displacement at node no. J; R_{resJ} is the resultant force in the insulator no J; L_0 is the conductor length that is calculated as $L_0=L_x.(1+8/3.(sag/L_x)^2)$; Q_{yn} is the shear force in span n due to the downburst load; d_{yN} is the y-displacement at node N.

$$C_n = \frac{L_0 \cdot \dfrac{1}{\sqrt{2}} \sqrt{\displaystyle\int_0^1 Q_{yn}(s)^{*2}\,ds + \dfrac{W^2 L_x^{\,2}}{12} + 2 \cdot \dfrac{T_n}{L_x}\left((dy_{N+1} - dy_N) \displaystyle\int_0^1 Q_{yn}(s)^*\,ds \right)}}{2\left(L_x + dx_{N+1} - dx_N\right)^2 \cdot \left(\dfrac{L_0}{L_x + dx_{N+1} - dx_N} - 1\right)^{3/2}}$$

Appendix B

Figures for the reaction time responses
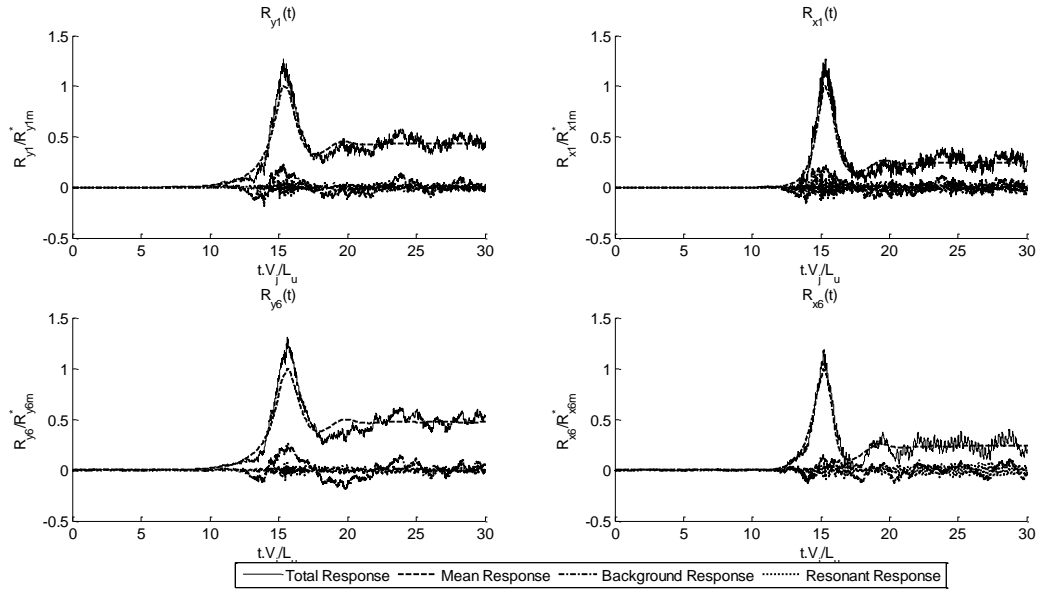
Fig. B1 Reaction Responses for Case 1 (Db$_x$, L$_x$=300 m, V$_{ref}$= 40 m/s)
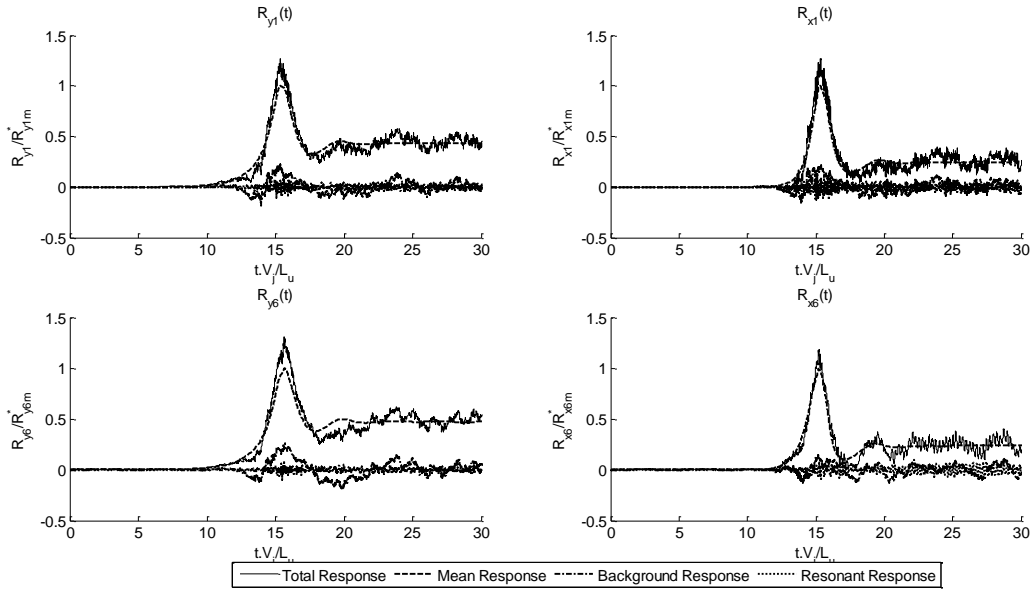
Fig. B2 Reaction Responses for Case 2 (Db$_x$, L$_x$=300 m, V$_{ref}$= 20 m/s)
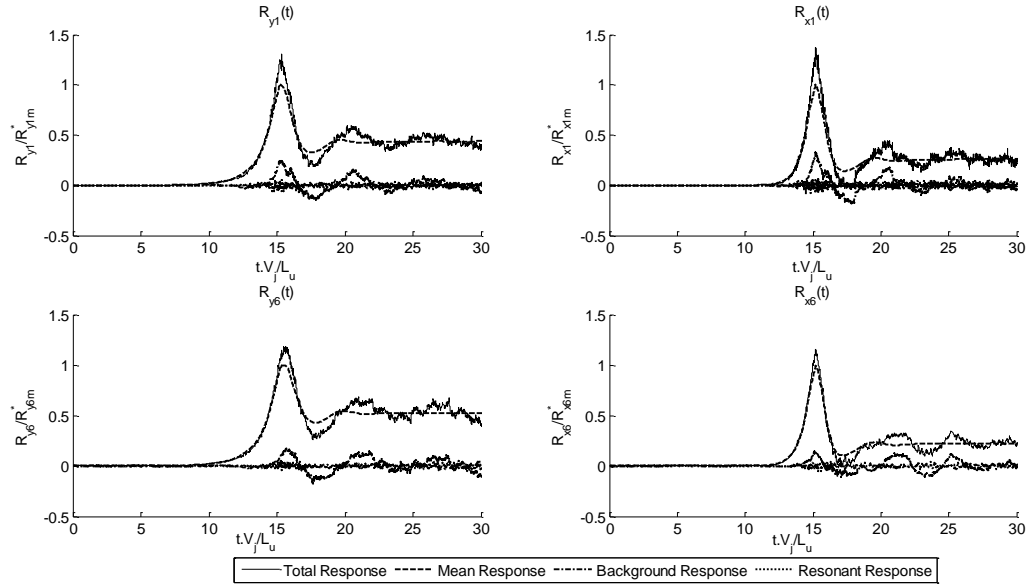
Fig. B3 Reaction Responses for Case 3 (Db$_x$, L$_x$=500 m, V$_{ref}$= 40 m/s)
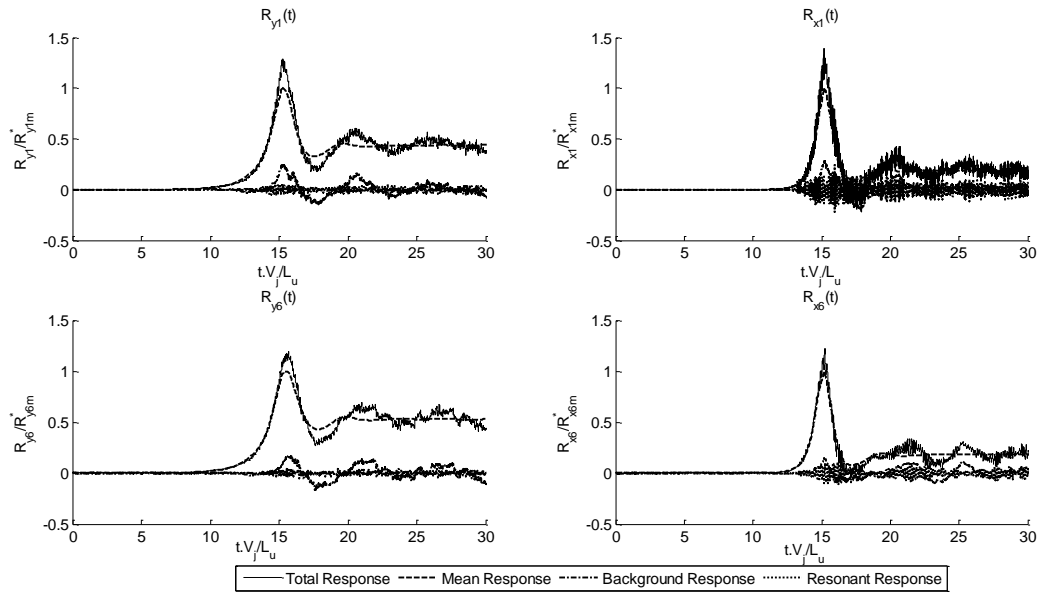
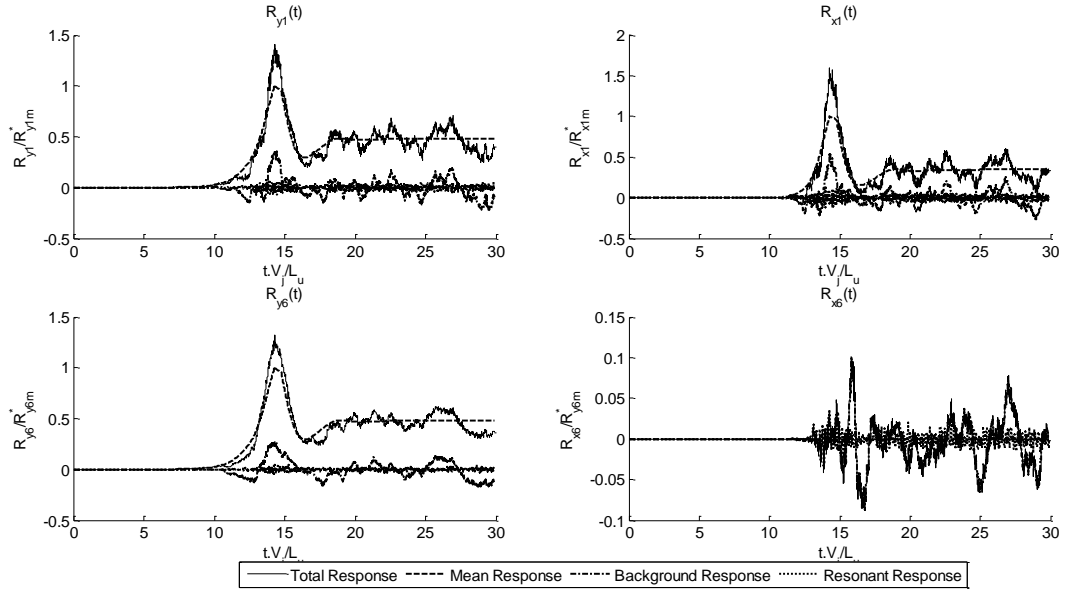Fig. B4 Reaction Responses for Case 4 (Db$_x$, L$_x$=500 m, V$_{ref}$= 20 m/s)

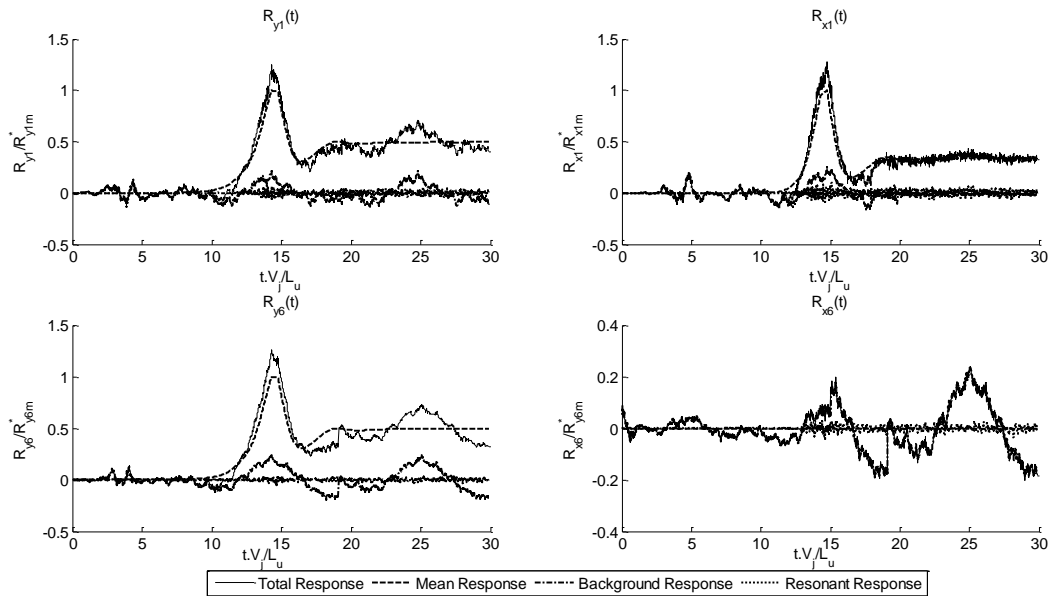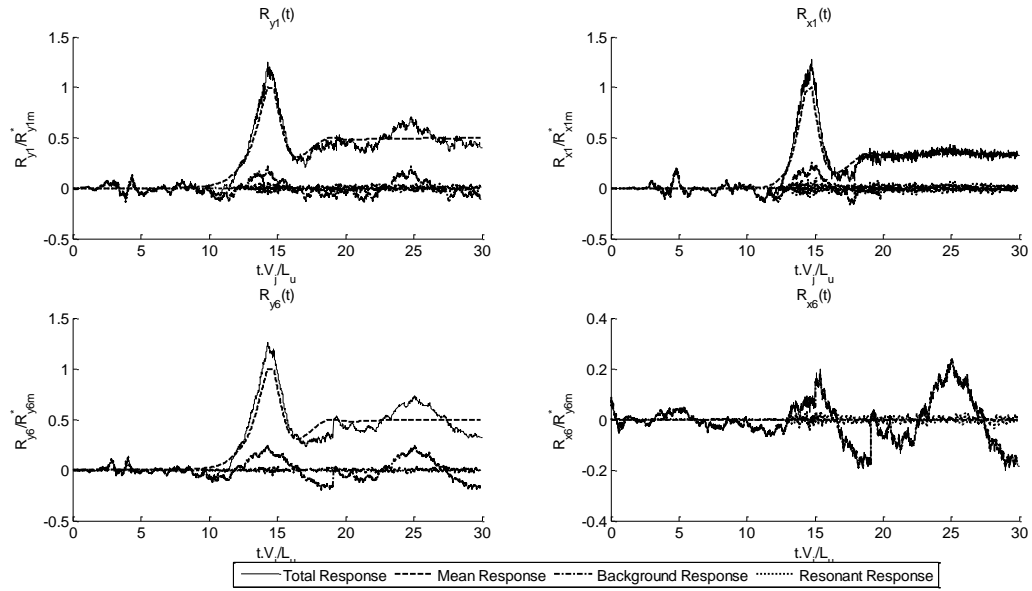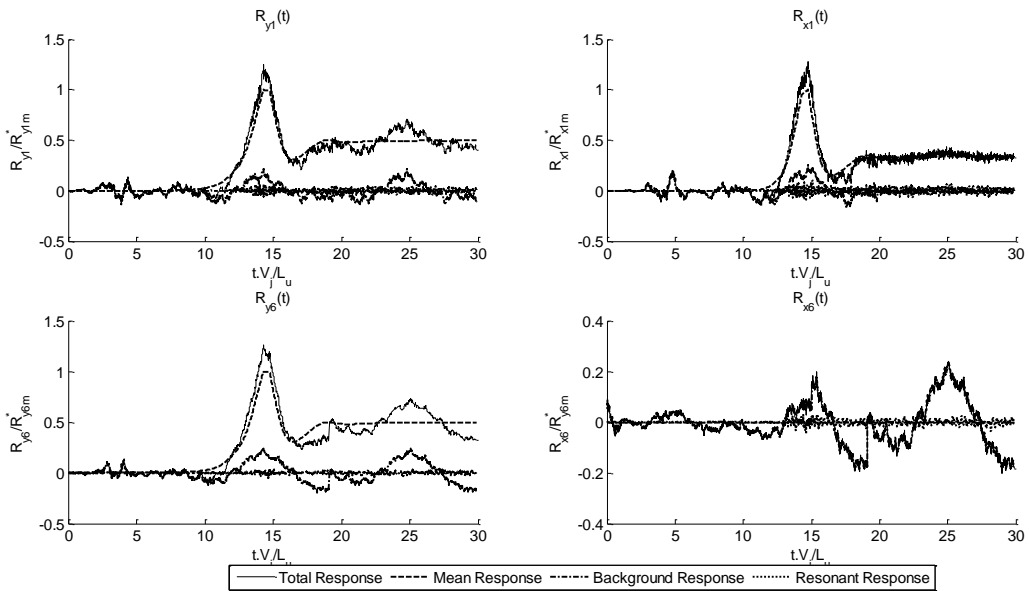Fig. B5 Reaction Responses for Case 5 (Db_y, L_x=300 m, V_{ref}= 40 m/s)

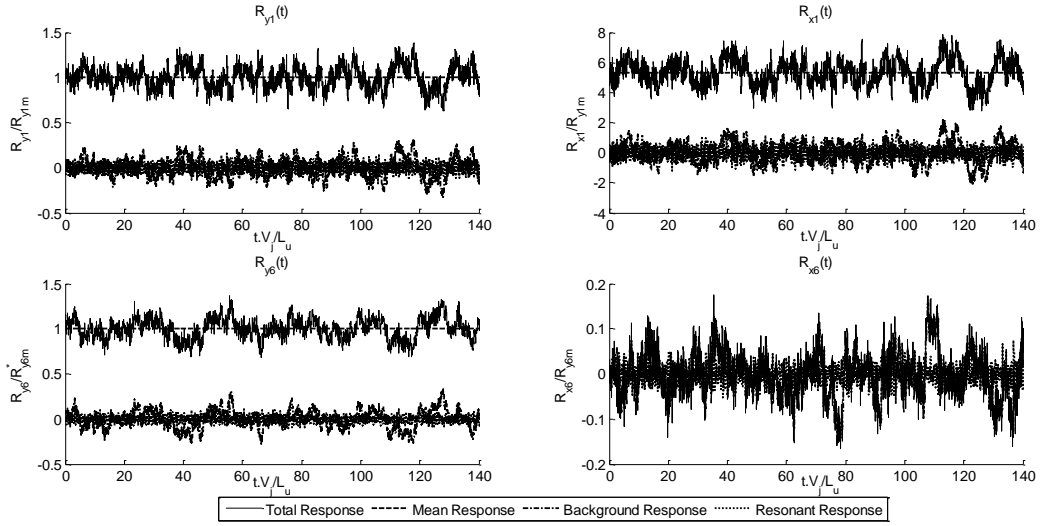Fig. B6 Reaction Responses for Case 6 (Db_y, L_x=300 m, V_{ref}= 20 m/s)

Fig. B7 Reaction Responses for Case 7 (Db$_y$, L$_x$=500 m, V$_{ref}$= 40 m/s)

Fig. B8 Reaction Responses for Case 8 (Db$_y$, L$_x$=500 m, V$_{ref}$= 20 m/s)

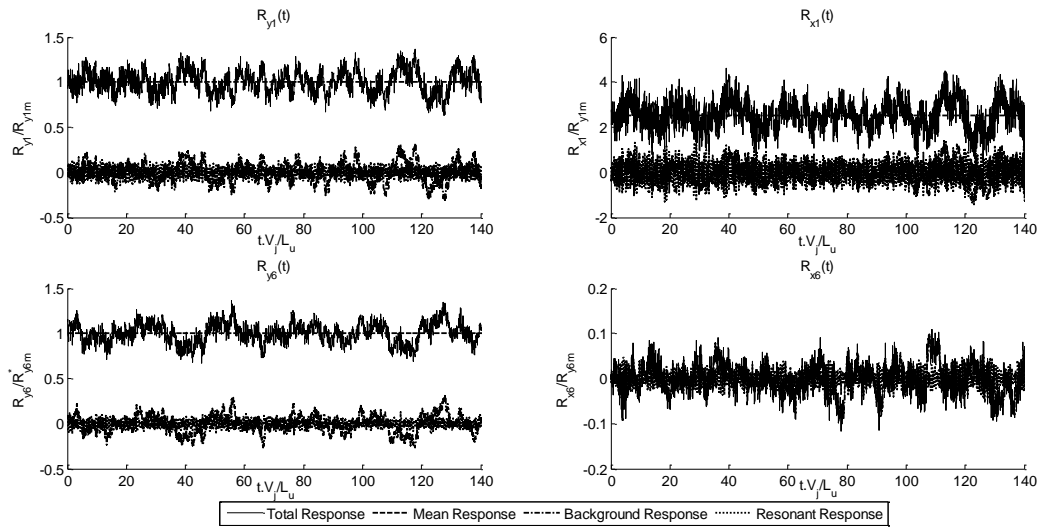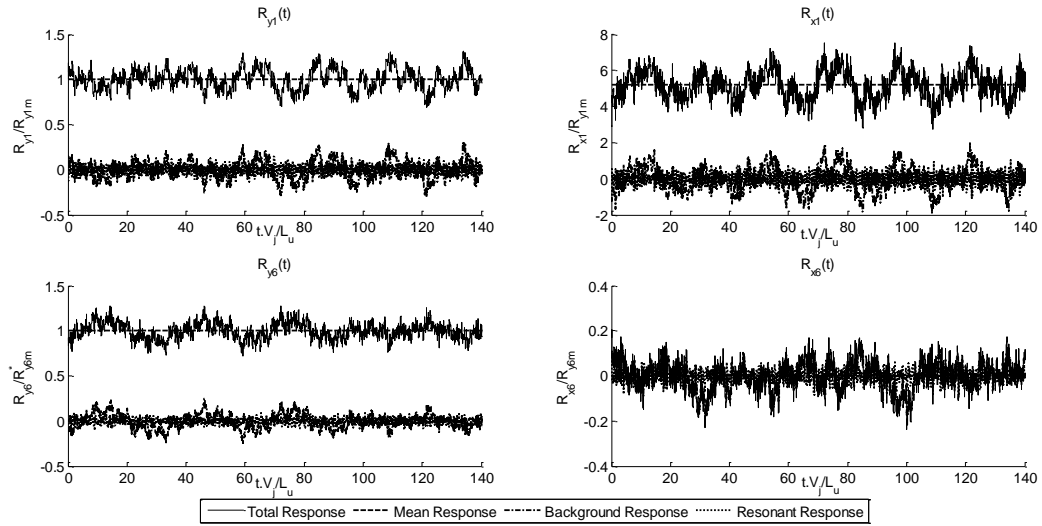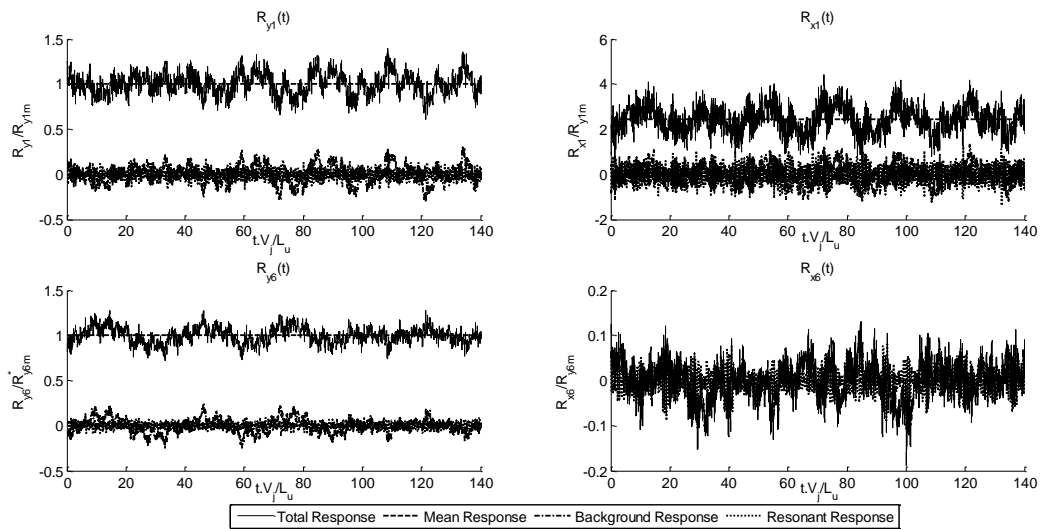Fig. B9 Reaction Responses for Case 9 (Sy L_x=300 m, V_{ref}= 40 m/s)

Fig. B10 Reaction Responses for Case 10 (Sy, L_x=300 m, V_{ref}= 20 m/s)

Fig. B11 Reaction Responses for Case 11(Sy, L_x=500 m, V_{ref}= 40 m/s)

Fig. B12 Reaction Responses for Case 12 (Sy, L_x=500 m, V_{ref}= 20 m/s)